

A. LENGWENUS¹
J. KRUSE¹
M. VOLK^{1,*}
W. ERTMER²
G. BIRKL^{1,✉}

Coherent manipulation of atomic qubits in optical micropotentials

¹ Institut für Angewandte Physik, Technische Universität Darmstadt, Schlossgartenstr. 7, 64289 Darmstadt, Germany

² Institut für Quantenoptik, Universität Hannover, Welfengarten 1, 30167 Hannover, Germany

Received: 9 August 2006

Published online: 20 December 2006 • © Springer-Verlag 2006

ABSTRACT We experimentally demonstrate the coherent manipulation of atomic states in far-detuned dipole traps and registers of dipole traps based on two-dimensional arrays of microlenses. By applying Rabi, Ramsey, and spin-echo techniques, we systematically investigate the dephasing mechanisms and determine the coherence time. Simultaneous Ramsey measurements in up to 16 dipole traps are performed and prove the scalability of our approach. This represents an important step in the application of scalable registers of atomic qubits for quantum information processing. In addition, this system can serve as the basis for novel atomic clocks making use of the parallel operation of a large number of individual clocks each remaining separately addressable.

PACS 03.67.Lx; 32.80.Pj; 42.50.-p

1 Introduction

In recent years, there has been growing interest in the experimental realization of scalable configurations for quantum information processing [1, 2]. Approaches based on neutral atoms in microscopic trapping potentials offer a promising combination of scalability, high decoupling from environmental sources of decoherence, and advanced techniques for the manipulation of internal and external degrees of freedom. Trapping can be achieved either by electric and magnetic potentials created by micro-fabricated charge- or current-carrying structures [3, 4], or by optical dipole potentials in the form of single traps [5], interfering laser beams (optical lattices) [6–8] or by light fields tailored by micro-fabricated optical elements [9].

In our work, we employ micro-fabricated arrays of diffractive or refractive lenses to create two-dimensional registers of dipole traps (Fig. 1). In the individual traps, we store neutral rubidium (⁸⁵Rb) atoms in order to generate two-dimensional registers of quantum bits (qubits) encoded in the internal or external states of the atoms. We have already demonstrated the preparation of up to 80 qubit ensembles trapped in par-

allel, the individual addressability of each register site, the controlled preparation of qubit states in each site, and the independent readout of the qubit state of each site [10].

In this paper, we present the next important step towards a functional quantum processor, namely the coherent manipulation of qubits encoded in internal atomic states, the investigation of dephasing, and the determination of the coherence time. One important feature is the demonstration that the coherent qubit manipulation and the corresponding readout of the result of this manipulation can be performed in a scalable fashion for a large number of sites of the qubit register in parallel.

2 Experimental setup

The experiments are performed with rubidium atoms prepared by laser cooling and trapping techniques. The experimental setup is depicted in Fig. 2. The central part is a glass cuvette ($22 \times 22 \times 52 \text{ mm}^3$) which is attached to the main vacuum system by a glass-to-metal adaptor. The pressure is kept below 1×10^{-9} mbar using an ion-getter pump. We control the partial pressure of rubidium by either switching on two dispensers in the vacuum chamber, or by illuminating the glass cell with UV-light at 395 nm emitted by an array of high intensity LEDs. While the UV-light is on, atoms which had been adsorbed at the surface of the glass cell can desorb and defuse into the vacuum, thereby increasing the partial pressure of rubidium [11]. We capture and precool atoms in a magneto-optical trap (MOT) which has a magnetic field in anti-Helmholtz configuration with a gradient of 14 Gauss/cm along the symmetry axis. Three retroreflected laser beams, which are orthogonal in orientation and red-detuned by two linewidths relative to the $5S_{1/2}, F = 3 \rightarrow 5P_{3/2}, F = 4'$ transition, complete the MOT setup. The total power of the three incoming cooling beams is about 2 mW, where each beam has a waist of about 3.5 mm. Repumping light resonant to the $5S_{1/2}, F = 2 \rightarrow 5P_{3/2}, F = 3'$ transition pumps atoms from the $F = 2$ groundstate back into the cooling cycle. The glass cell is anti-reflection coated on the outside to maximize transmission of the cooling and repumping beams of the magneto-optical trap.

We trap atoms either in arrays of optical dipole traps or – for systematic studies – in single traps. To create trap arrays, we employ the setup shown in Fig. 2. A microlens array (see Sect. 5 for details) is illuminated by a collimated linear polarized Gaussian laser beam from a titanium sapphire

✉ Fax: +49-5161-162410,
E-mail: gerhard.birkel@physik.tu-darmstadt.de

*Present address: Swinburne University of Technology, Melbourne, Australia

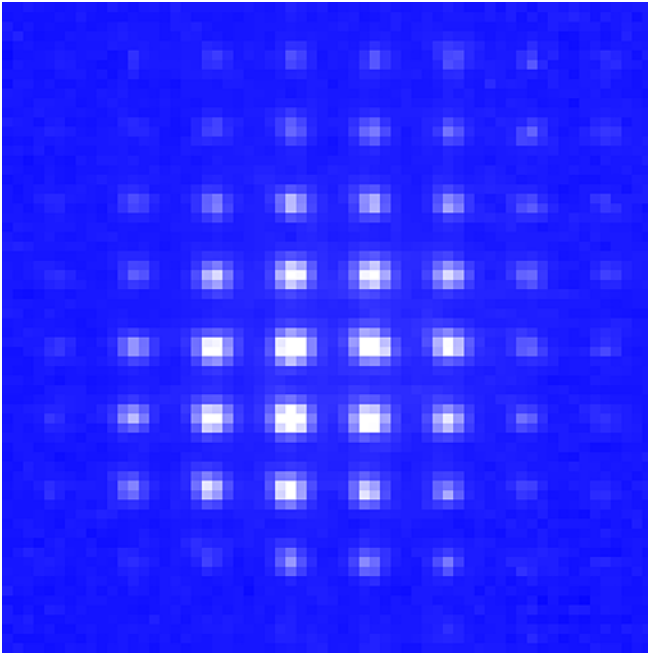


FIGURE 1 Fluorescence image of about 50 atom samples trapped in a two-dimensional array of dipole traps. The traps have a waist of $1.7 \mu\text{m}$ and are separated by $54 \mu\text{m}$. The central trap contains several $100 \text{ }^{85}\text{Rb}$ atoms

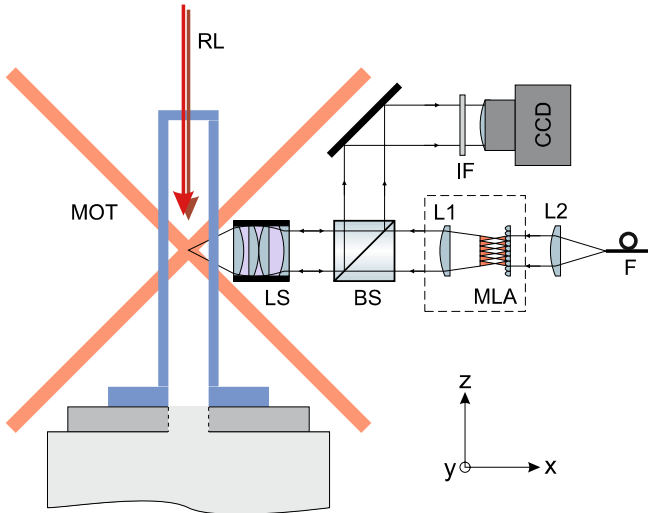


FIGURE 2 Experimental setup for trapping atoms in arrays of dipole traps (not to scale). A micro-lens array (MLA) is illuminated by the light of a TiSa laser delivered by an optical fiber (F). The focal plane of the lens array is transferred by lens (L1) and lens system (LS) into the MOT-region. Fluorescence of the atoms is detected in the reverse direction: behind the lens system (LS) the light is separated by a polarizing beamsplitter (BS) and imaged onto a CCD chip. The Raman lasers (RL) enter through the end surface of the cell

laser (TiSa). The laser light has a wavelength of 815 nm and is therefore red-detuned from the D1 and the D2 line with an effective detuning of $\delta_{\text{eff}}/2\pi = -13.04 \text{ THz}$. The focal plane of the array is projected into the glass cell by a telescope. The telescope consists of an achromatic lens ($f = 80 \text{ mm}$) and a diffraction limited lens system with a working distance of 36 mm . This creates arrays of dipole traps with a waist of $1.7 \mu\text{m}$ ($1/e^2$ radius) and a separation of $54 \mu\text{m}$. Experiments on a single trap are either performed by selecting one trap out of the array or by removing the micro-lens array (MLA) and

the transfer lens (L1). The latter case results in a single dipole trap with a waist of $9.7 \mu\text{m}$. For detection, we illuminate the atoms with the cooling and repumping beams for $300 \mu\text{s}$. The fluorescence light is collected with lens system LS and then reflected by a polarizing beamsplitter onto an electron multiplying charge coupled device camera (EMCCD). The advantage of this type of camera is the electron multiplication directly on the CCD chip which is comparable to the performance of an avalanche photodiode. Hence, readout noise is minimized, which enables us to detect even single photons. An interference filter (IF) placed in front of the camera blocks straylight from the TiSa, while transmitting fluorescence light at 780 nm .

3 Experimental sequence

A typical experimental sequence is as follows: first, the MOT is loaded from the background gas by switching on the magnetic field and the cooling and repumping beams. After the MOT is loaded, the atoms are further cooled for 5 ms by polarization gradient cooling. During this period, the TiSa beam is switched on by an acousto-optical modulator, and atoms are loaded into the dipole trap, which is superimposed on the MOT and the optical molasses. Switching off the MOT beams and waiting for another 50 ms ensures that all atoms not trapped in the dipole trap have left the detection region. The number of loaded atoms is on the order of 1000 atoms per trap. The temperature is measured by a time-of-flight method and is approximately $40 \mu\text{K}$.

3.1 Qubit preparation and state selective detection

After the atoms have been loaded into the dipole trap, they have to be initialized for coherent manipulation. We have chosen the hyperfine states $|0\rangle \equiv |F=2, m_F=0\rangle$ and $|1\rangle \equiv |F=3, m_F=0\rangle$ as qubit states, because of their insensitivity to fluctuations of the magnetic field. This specific choice is only possible in dipole traps not relying on the Zeeman shift for atom trapping. As an important consequence, we can coherently manipulate the qubit states by driving the in first-order magnetic field insensitive clock transition $|F=2, m_F=0\rangle \rightarrow |F=3, m_F=0\rangle$. However, we have to use a more elaborate optical pumping scheme to transfer the atoms into the $|F=3, m_F=0\rangle$ state for initialization, after being equally distributed over all seven m_F -states at the end of the loading phase from the MOT. For the pumping process we first switch off the cooling laser beams and apply a magnetic offset field of $50 \mu\text{T}$ (0.5 Gauss) along the z -axis to define a quantization axis. The pumping is induced by a π -polarized laser beam, which is resonant to the $|5S_{1/2}, F=3\rangle \rightarrow |5P_{3/2}, F'=3\rangle$ transition and the MOT repumping light to prevent pumping into the $|F=2\rangle$ state. For π -polarized light the $|F=3, m_F=0\rangle$ state is a dark state, so that atoms which end up in this state stay there during the pumping process. The efficiency of this pumping process is shown in Fig. 3 for atoms in the central trap of a dipole trap array with a trap depth of $k_B \times 1.0 \text{ mK}$ as well as for free expanding atoms (i.e. released from the MOT). We observe a pumping efficiency of up to 100% for free expanding atoms and an efficiency of 51% for atoms in the dipole potential with 49% of the atoms distributed over the $|F=3, m_F \neq 0\rangle$ states. We assume that the

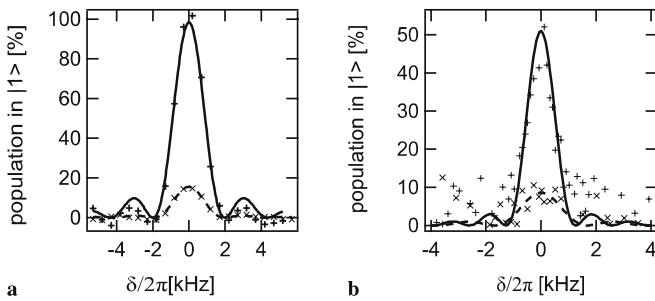


FIGURE 3 Efficiency of optical pumping: population in state $|1\rangle$ normalized to all atoms for (a) free expanding atoms and (b) atoms in the central trap of a dipole trap array. Fits to the central resonance (lines) are given for data (crosses) with (straight line) and without (dashed line) optical pumping. The functional form of the fits is given by the Fourier spectrum of a rectangular pulse used during detection (see Sect. 3.2 for details)

reduced efficiency in the dipole trap results from two photon transitions coupling the various $|m_F\rangle$ -states or from the Stark shift inside the dipole traps.

State selective detection is performed by using an additional intense laser pulse resonant to the $|F = 3\rangle \rightarrow |F' = 4\rangle$ transition. If the intensity is chosen to be sufficiently high ($I/I_0 \approx 100$), the radiation pressure force is stronger than the dipole force. The atoms in $|F = 3\rangle$ are then pushed out of the dipole trap so that only the atoms in $|F = 2\rangle$ remain.

One has to ensure that the irradiation time is short enough ($< 300 \mu\text{s}$), so that spontaneous decay into the $|F = 2\rangle$ state can be neglected. The atoms in $|F = 2\rangle$ are detected by resonant excitation with the MOT and repumping light and collecting the fluorescence light with the CCD camera. Note that this detection mechanism is not only state selective, but also resolves the atoms in space so that many traps can be detected at the same time. In combination with the spatial selective addressability demonstrated in [10], this presents a powerful scheme for preparation and readout of qubit states for scalable quantum information processing.

3.2 Coherent manipulation

We use a Raman laser system to coherently couple states $|0\rangle$ and $|1\rangle$. The Raman laser system consists of two phase locked extended cavity diode lasers with a frequency difference equal or close to the hyperfine splitting of the $5S_{1/2}$ state (3.04 GHz). The output radiation can be switched by an acousto-optical modulator. If we illuminate atoms which are prepared in the upper qubit state $|1\rangle$ with Raman pulses of variable length, periodic transfer of the population to and from the lower qubit state $|0\rangle$ occurs. Here, we make use of the fact that the magnetic offset field shifts transitions between other magnetic substates out of resonance. Therefore, atoms not pumped into $|1\rangle$ during preparation do not contribute to the subsequent population transfer. Rabi oscillations of atoms in one of the central traps of a dipole trap array are shown in Fig. 4. The trap depth is $k_B \times 1.2 \text{ mK}$. Each data point represents a separate Rabi experiment with differing duration of the Raman pulse. Measured populations are normalized to the number of trapped atoms before optical pumping.

Fluctuations in the measured population are mostly of a statistical nature and occur mainly due to fluctuations of the number of loaded atoms and imperfect efficiency in prepar-

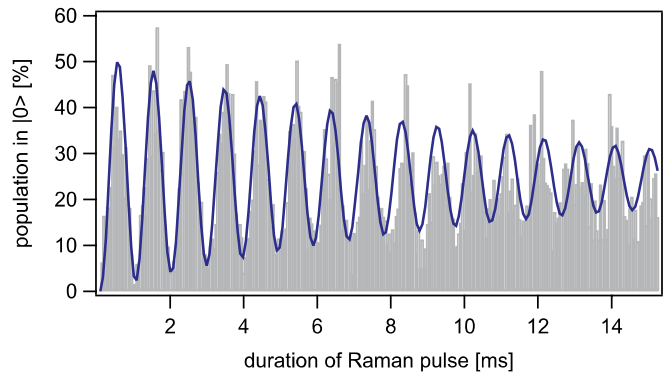


FIGURE 4 Rabi oscillations in a dipole trap: population of the state $|0\rangle$ normalized to all atoms in the trap before optical pumping as a function of the duration of the Raman pulse. 98% of the atoms prepared in state $|1\rangle$ participate in the first Rabi cycle

ation and detection. We fit the solution of the numerically integrated Bloch equations to the data by taking into account that due to spontaneous scattering of photons from the trapping beam the population in the initially empty state $|0\rangle$ increases with time. We find that 50% of the trapped atoms participate in the Rabi oscillations. Including the pumping efficiency of 51% (see Fig. 3b), we find that 98% of the atoms prepared in $|1\rangle$ contribute to the Rabi oscillations.

From the fit we determine a Rabi frequency of $\Omega_R = 2\pi \times (995 \pm 5) \text{ s}^{-1}$. The damping of the oscillations is caused by dephasing and decoherence effects. Both effects are indistinguishable in this measurement. We will focus on dephasing and decoherence effects in the following section. Maximum coherent population transfer can be achieved by irradiating the atoms with a resonant Raman pulse of length $\pi/\Omega_R = (503 \pm 3) \mu\text{s}$ (π -pulse). Such a pulse is employed to pump atoms from $|1\rangle$ to $|0\rangle$ with high efficiency during the state-selective detection sequence. Varying the frequency difference of the Raman laser fields gives the frequency dependent transfer efficiency shown in Fig. 3.

4 Dephasing and coherence

A real quantum mechanical system cannot be perfectly isolated from the environment. This will cause an initial pure quantum state to evolve into a statistical mixture of states which manifests itself in two effects, namely dephasing and decoherence. These effects are responsible for information loss in a quantum system. Long coherence times are therefore a crucial parameter for the applicability of a physical system for quantum information processing. We follow the previously discussed methods to study decoherence of quantum states of neutral atoms in optical dipole traps [12–14].

A theoretical description of these effects can be based on the Bloch equations [15]:

$$\dot{u} = -\delta v - \frac{u}{T_2}, \quad (1a)$$

$$\dot{v} = \delta u - \Omega_R w - \frac{v}{T_2}, \quad (1b)$$

$$\dot{w} = \Omega_R v - \frac{w - w_{\text{eq}}}{T_1}. \quad (1c)$$

The notation is taken from nuclear magnetic resonance (NMR) physics. T_1 is called longitudinal relaxation time and describes the time constant in which the inversion w of the system evolves to its equilibrium value w_{eq} . This can be caused by scattering of photons from the trapping laser or by collisions and can be equated to the coherence time. The transversal relaxation time T_2 describes the change in polarization u and v of the system. It is composed of an irreversible polarization decay time T_2' (homogeneous dephasing) and a reversible part T_2^* (inhomogeneous dephasing):

$$\frac{1}{T_2} = \frac{1}{T_2'} + \frac{1}{T_2^*}. \quad (2)$$

4.1 Ramsey measurements

In the Rabi experiment, oscillations are driven with the Raman lasers continuously illuminating the atoms during the period of coherent manipulation. This can cause scattering of photons from the Raman light fields as well as a differential light shift of the qubit states. While the first effect will destroy coherence the second effect shifts the transition frequency, which affects the inhomogeneous dephasing time T_2^* . One can overcome these problems by extending the Rabi experiment to a Ramsey experiment [16]. We first prepare the atoms in the state $|1\rangle$ as before. A $\pi/2$ -pulse transfers them to a coherent superposition of the two qubit states $|1\rangle$ and $|0\rangle$. In the framework of the Bloch model (1), the Bloch vector is flipped into the equatorial plane (uv -plane). Now, the Raman pulses are switched off, which results in a free precession of the Bloch vector around the w -axis. The angular frequency $\delta = \omega_{\text{Atom}} - \omega_{\text{RL}}$ is given by the frequency difference between the present atomic resonance (generally shifted from the nominal hyperfine splitting of the $5S_{1/2}$ state with $\omega_{\text{HFS}} = 3.0357$ GHz) and the frequency difference of the Raman lasers. For resonant pulses ($\omega_{\text{RL}} = \omega_{\text{HFS}}$), δ is mainly given by the differential light shift induced by the dipole trap and the quadratic Zeeman shift by the magnetic offset field. After free precession during time t , a second $\pi/2$ pulse is applied which rotates the Bloch vector by 90 degrees around the u -axis. Finally, detection gives the population in the lower qubit state $|0\rangle$. Without any dephasing or decoherence, this results in an oscillation of the probability $P_{|0\rangle}$ of finding the atom in the state $|0\rangle$ depending on the free precession time

$$P_{|0\rangle} = \frac{1-w}{2} = \frac{1}{2} (1 + \cos \delta t). \quad (3)$$

Taking into account that we are working with an ensemble of atoms which are thermally distributed in the dipole trap one can follow the calculations in [14] giving

$$P_{|0\rangle}(t) = A\alpha(t, T_2^*) \cos[\delta t + \kappa(t, T_2^*) + \Phi] + C, \quad (4)$$

where

$$\alpha(t, T_2^*) = \left[1 + 0.95 \left(\frac{t}{T_2^*} \right)^2 \right]^{-3/2}, \quad (5a)$$

$$\kappa(t, T_2^*) = -3 \arctan \left(0.97 \frac{t}{T_2^*} \right). \quad (5b)$$

If we assume that the thermal distribution of the atoms is the dominating cause of inhomogeneous dephasing, one gets a relation between the dephasing time T_2^* and the mean temperature T of the atomic ensemble

$$T = 1.94 \frac{\hbar \delta_{\text{eff}}}{k_B \omega_{\text{HFS}} T_2^*}. \quad (6)$$

Because of its specific kinetic energy, every atom in a thermal ensemble experiences a different shift δ in the dipole trap due to the fact that for the lower qubit state $|0\rangle$ the detuning of the dipole trap is larger by ω_{HFS} than for the upper qubit state $|1\rangle$ (differential light shift). For example, atoms with lower temperature will be found more at the bottom of the trap and will therefore experience a larger differential light shift. In the Bloch model, this is equivalent to a different precession frequency of the Bloch vectors around the w -axis. If an ensemble of atoms is considered, the Bloch vectors of all atoms will spread out leading to a reduced visibility of the Ramsey signal. Equation (4) also embodies the constant offset A and C , which are relevant for fitting experimental data, because they account for the actual population in the upper and lower qubit states. The phase offset Φ accounts for an additional phase shift the system gains since the Bloch vector not only precesses during the free evolution time t but also during the $\pi/2$ -pulses.

We investigated Ramsey oscillations in the single dipole trap setup. The results are depicted in Fig. 5. Clearly observable are Ramsey oscillations with precession frequency δ and a reduction of the modulation amplitude of the signal with increasing t . The precession frequency is determined by $\delta = \delta_{\text{RL}} + \delta_{\text{shift}}$ where $\delta_{\text{RL}} = \omega_{\text{RL}} - \omega_{\text{HFS}}$ is the detuning of the Raman lasers from the frequency of the hyperfine splitting. Additional shifts acting on the atomic states are summarized in δ_{shift} which are mainly the differential light shift and the quadratic Zeeman shift. Due to the high spectroscopic resolution of the Ramsey technique, we can directly measure δ_{shift} as a function of external parameters.

Figure 6 visualizes the measured resonance shift δ_{shift} as a function of trap depth. Typical trap depths range from $k_B \times 200 \mu\text{K}$ to $k_B \times 400 \mu\text{K}$. We calculate the frequency shift using a Raman laser detuning of $\delta_{\text{RL}} = 0$ and a quadratic Zeeman shift, which is induced by the magnetic offset field of $50 \mu\text{T}$ (0.5 Gauss). This gives a frequency offset of $\delta_{\text{shift}}(0) \approx +320$ Hz in the absence of the dipole trap. The solid line in Fig. 6 represents the calculated shift which agrees well with our data. From this and similar measurements, we know that we can determine frequency shifts for atoms trapped in the dipole potential with a spectroscopic resolution of better than 100 Hz.

4.2 Echo measurements

It is not possible to determine the coherence time based on Ramsey measurements. As already explained, the decay of the signal can also be caused by dephasing, so that decoherence effects are not distinguishable from dephasing effects. In order to check whether the dominating dephasing mechanism is reversible and to determine the coherence time of the system, one can extend the Ramsey measurements to (spin-)echo-spectroscopy [17, 18]. Echo measurements with

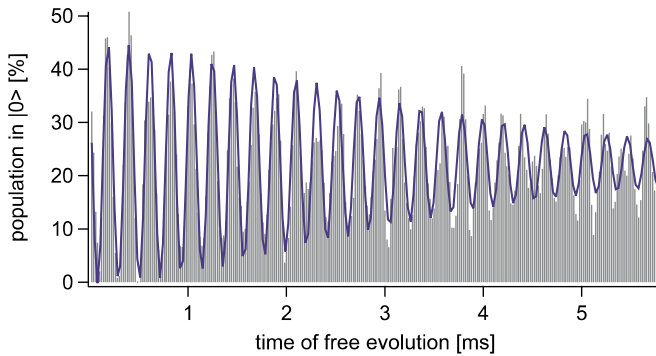


FIGURE 5 Ramsey measurement in a single dipole trap. From the fit we get a dephasing time $T_2^* = (4.08 \pm 0.22)$ ms and a precession frequency of $\delta = 2\pi \times (4814 \pm 5)$ Hz

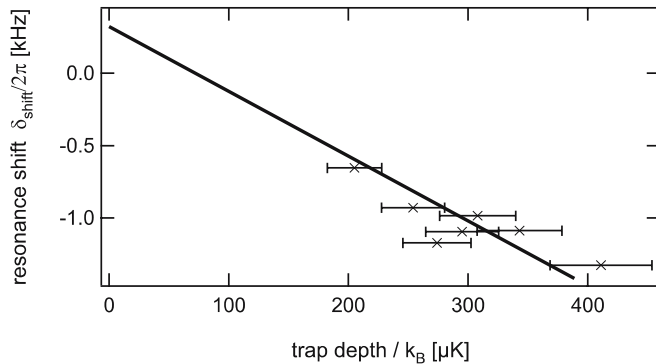


FIGURE 6 Shift δ_{shift} of the atomic resonance as a function of trap depth. Experimental data from Ramsey measurements are compared to theory (line) which takes into account the differential light shift and the quadratic Zeeman effect

atoms in optical dipole potentials have already been presented in [19, 20]. The idea is to reverse the dephasing which occurs after the first $\pi/2$ -pulse at $t_0 = 0$ by applying an additional π -pulse at $t_1 > t_0$. This will lead to a new maximum in the modulation amplitude at time $t = 2t_1$. A typical echo measurement together with the corresponding Ramsey measurement and theoretical fits is shown in Fig. 7 for a time $t_1 = 7.5$ ms. This measurement was performed in the single trap setup. As expected, the signal modulation is again maximized at a time corresponding to the echo signal with a modulation amplitude significantly larger than for the Ramsey experiment after the same time delay. This is proof that the reduction of the Ramsey fringes is dominated by dephasing and not by decoherence. The visibility of the echo signal, which is defined as the amplitude of modulation of the echo signal at $t = 2t_1$ relative to the amplitude of modulation of the Ramsey signal at $t = 0$, gives information about decoherence and homogeneous dephasing. The visibility as a function of increasing t_1 is shown in Fig. 8. A reduction of the visibility being due to decoherence caused by spontaneous scattering of photons should lead to an exponential visibility decay with a time constant given by the inverse photon scattering rate. An exponential fit to the data in Fig. 8 results in a decay time of $T_{\text{echo}} = (68.0 \pm 7)$ ms.

This value agrees well with the inverse spontaneous scattering rate from the trapping laser light which is $\Gamma_{\text{sc}}^{-1} = (68.0 \pm 5)$ ms. From this we draw the conclusion that the reduction of the echo visibility is a result of spontaneous scattering of photons from the trapping light. Thus, the echo

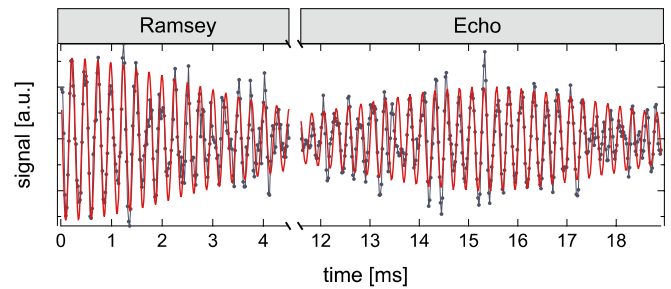


FIGURE 7 Ramsey and echo measurement in a dipole trap together with a theoretical fit. The π -pulse which reverses the dephasing is applied at $t_1 = 7.5$ ms. After $2t_1 = 15$ ms the modulation of the signal is again maximized

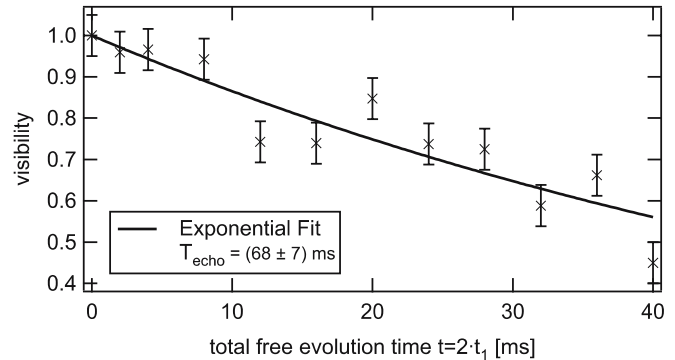


FIGURE 8 Visibility of the echo signal at $t = 2t_1$. Assuming that decoherence caused by spontaneous scattering is the main cause for loss of visibility, the data can be fitted by an exponential decay (line)

measurement directly gives the coherence time $T_1 \approx T_{\text{echo}}$. Although homogeneous dephasing might be present, the time constant for T_2' should be significantly larger than the time constant for decoherence T_1 . As a consequence, it should be possible to further increase the coherence time by increasing the detuning of the trapping laser.

5 Simultaneous Ramsey measurements

Two-dimensional registers of qubits in arrays of dipole traps based on microoptical elements are central for our implementation of quantum information processing with cold neutral atoms. It is essential to demonstrate the applicability of the techniques described in the previous sections to atoms trapped in dipole trap arrays. This includes the demonstration of parallel qubit manipulation and a scheme for simultaneous but also site-specific detection of the outcome of the respective operations.

For this purpose, we performed a simultaneous Ramsey experiment on 16 atom samples trapped in a 4×4 array of dipole traps with a readout of the results based on position resolved imaging. The dipole traps are based on a diffractive array of microlenses with a total of 50×50 lenses. The lenses are separated by $125 \mu\text{m}$ and have a nominal focal length of $625 \mu\text{m}$. The array is illuminated by a linear polarized titanium sapphire laser beam with a power of 130 mW and wavelength of 800 nm.

Due to the limited diffraction efficiency, about 40% of the incident light contribute to dipole trapping. The focal plane of the array is imaged onto the MOT by a telescope which con-

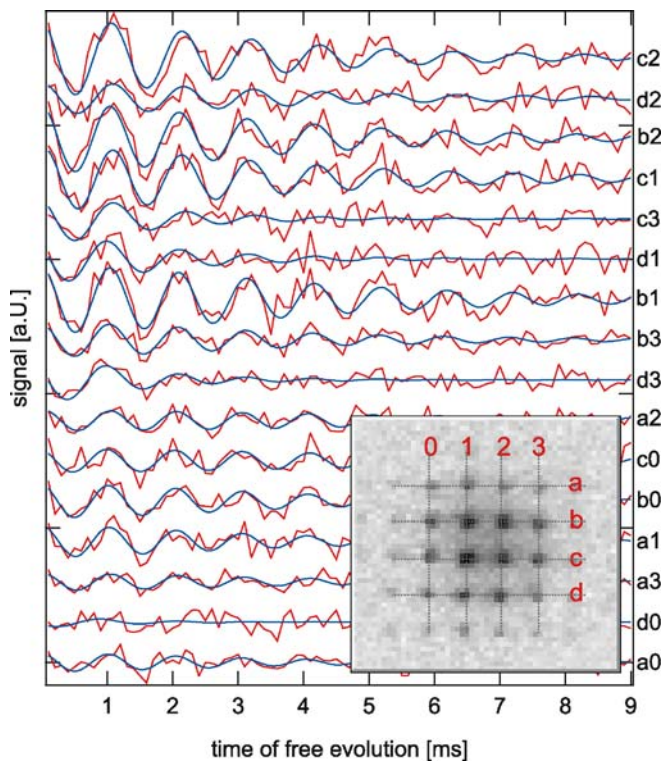


FIGURE 9 Simultaneous Ramsey measurements in 16 different dipole traps. The associated position of the traps is shown in the inset. The inset is a fluorescence image of the atoms trapped in the two-dimensional trap array

sists of an achromat with a focal length of 80 mm and the lens system with a working distance of 36 mm. The trap array is resized to a distance between foci of $54\ \mu\text{m}$. We measured the waists of each trap at the position of the MOT to $1.7\ \mu\text{m}$. Due to the Gaussian shape of the incident beam illuminating the lens array, the depths of the dipole traps vary from outer to inner traps with $k_B \times 600\ \mu\text{K}$ for the weakest and $k_B \times 1.2\ \text{mK}$ for the deepest traps.

After loading the atoms from the MOT, we end up with more than 16 filled traps with around 500 atoms in the central trap. The population of the outer traps is reduced by more than one order of magnitude because of the lower trap depth and the inferior overlap with the optical molasses. The temperature of the atom ensembles in the traps was determined to be less than $50\ \mu\text{K}$. The previous mentioned techniques for coherent manipulation are simply applicable to the trap array by illuminating all traps with Raman laser light simultaneously. Also the detection scheme is fully adoptable to trap registers: we perform the readout of the final result by taking spatially resolved images of fluorescence emitted by the atoms (see inset in Fig. 9). The images are analyzed by integrating the fluorescence around each known position of an atom sample and thus achieving a site-specific determination of the population of the qubit states at each site. Figure 9 shows simultaneous Ramsey measurements for 16 register sites. Clearly visible are Ramsey oscillations in almost all of the atom samples. The variation in signal strength reflects the variation in atom number. This proves that parallel coherent manipulation has been achieved. Together with the site-specific addressability as presented in [10] this is a clear demonstration of the scalability of our system and the tech-

niques used for preparing, manipulating, and readout of the qubit states.

6 Conclusion and outlook

With this work, we have systematically studied the coherent manipulation of atomic qubits in optical micropotentials based on individual dipole traps and trap arrays. By applying a range of techniques, like Rabi, Ramsey, and spin-echo techniques, we could investigate dephasing and decoherence of atomic qubits in dipole traps. We could show that our approach for quantum information processing based on trapping atomic qubits in arrays of dipole traps allows for a simultaneous coherent manipulation of a large number of atomic qubits. This presents an important step towards the realization of a scalable quantum processor with atomic qubits. With the results described in this paper ($\pi/2$ times of approx. $250\ \mu\text{s}$ and a coherence time of 68 ms) we already can perform more than 100 single qubit gate operations within the coherence time. In addition, this value can be significantly increased: so far decoherence is given by the inverse of the spontaneous scattering rate of the trapping light. This rate can be reduced by increasing the detuning of the trapping light. For traps based on the light of a Nd:YAG laser (or similar) at around 1064 nm, decoherence times in excess of 1 s are achievable for comparable trap depths. In addition, for the measurements presented above the light of the Raman laser was distributed over a size of about $1\ \text{cm}^2$ in order to illuminate all trapping sites homogeneously. As the next step, this light can be concentrated onto the known sites of the atom samples. This will allow increasing of the intensity of the Raman light by more than a factor of 100 thus reducing the $\pi/2$ time to a value well below $10\ \mu\text{s}$. With these two measures the number of single qubit gate operations can be increased to a value of more than 10^5 during the coherence time, bringing the system into the parameter range necessary for complex quantum gate schemes and the implementation of quantum error correction codes.

One of our current projects is the demonstration of a detection sensitivity down to one atom per register site. Estimates based on the known parameters of the detection scheme and the specifications of the CCD camera together with initial experiments on the current detection limit allow us to expect that single atom detection is possible in the setup described in this work. This will allow opening of work in an additional direction: a two-dimensional array of well separated trapped single atoms can serve as an excellent basis for a new scheme of atomic clocks. In recent work, the applicability of atoms in optical lattices [21] and microchip traps [22] as a frequency reference has been discussed. For optical traps, using trapping light at a so called ‘magic’ wavelength (as is possible for strontium) minimizes the effect of differential light shifts on the frequency of the clock transition. For ^{85}Rb , it was shown that an additional light field tuned between the two hyperfine ground states can also be used to suppress the differential light shift [23]. Combining these results with a trapping geometry based on arrays of microlenses would allow creation of a large register of single trapped atoms in a configuration where each atom can be spatially resolved. This allows treatment of each atom as an

individual atomic clock which can be separately observed, but at the same time gives a large number of individual clocks for increasing the signal-to-noise ratio or even making use of the superior performance of a massively entangled atom system.

ACKNOWLEDGEMENTS This work has been financially supported in part by the following funding organizations: DFG (Schwerpunktprogramm 'Quanteninformationsverarbeitung'), European Commission (IP 'ACQP', IP 'SCALA', RTN 'Atom Chips'), NIST/NSA/ARDA/DTO (QCCM Project 'Neutral Atom Quantum Computing with Optical Control'), and Land Hessen ('Innovationsbudget Quanteninformationverarbeitung').

REFERENCES

- 1 M.A. Nielsen, I.L. Chuang, *Quantum Computation and Quantum Information* (University Press, Cambridge, 2000)
- 2 T. Beth, G. Leuchs (Eds.) *Quantum Information Processing* (Wiley-VCH, Weinheim, 2005)
- 3 For an overview see: E.A. Hinds, I.G. Hughes, *J. Phys. D Appl. Phys.* **32**, R119 (1999)
- 4 For an overview see: R. Folman, P. Krüger, J. Schmiedmayer, J. Denschlag, C. Henkel, *Adv. At. Mol. Opt. Phys.* **48**, 263 (2002)
- 5 N. Schlosser, G. Reymond, I. Protchenko, P. Grangier, *Nature (London)* **411**, 1024 (2001)
- 6 P.S. Jessen, I.H. Deutsch, *Adv. At. Mol. Opt. Phys.* **37**, 95 (1996)
- 7 I. Deutsch, P.S. Jessen, *Phys. Rev. A* **57**, 1972 (1998)
- 8 G. Grynberg, C. Robilliard, *Phys. Rep.* **355**, 355 (2001)
- 9 G. Birkel, F.B.J. Buchkremer, R. Dumke, W. Ertmer, *Opt. Commun.* **191**, 67 (2001)
- 10 R. Dumke, M. Volk, T. Mütter, F.B.J. Buchkremer, G. Birkel, W. Ertmer, *Phys. Rev. Lett.* **89**, 097903 (2002)
- 11 C. Klempt, T. van Zoest, T. Henninger, O. Topic, E. Rasel, W. Ertmer, J. Arlt, *Phys. Rev. A* **73**, 013410 (2006)
- 12 N. Davidson, H.J. Lee, C.S. Adams, M. Kasevich, S. Chu, *Phys. Rev. Lett.* **74**, 1311 (1995)
- 13 R. Ozeri, L. Khaykovich, N. Davidson, *Phys. Rev. A* **59**, R1750 (1999)
- 14 S. Kuhr, W. Alt, D. Schrader, I. Dotsenko, Y. Miroshnychenko, A. Rauschenbeutel, D. Meschede, *Phys. Rev. A* **72**, 023406 (2005)
- 15 F. Bloch, *Phys. Rev.* **70**, 460 (1946)
- 16 N.F. Ramsey, *Phys. Rev.* **78**, 695 (1950)
- 17 E.L. Hahn, *Phys. Rev.* **80**, 580 (1950)
- 18 N.A. Kurnit, I.D. Abella, S.R. Hartmann, *Phys. Rev. Lett.* **13**, 567 (1964)
- 19 F.B.J. Buchkremer, R. Dumke, H. Levsen, G. Birkel, W. Ertmer, *Phys. Rev. Lett.* **85**, 3121 (2000)
- 20 M.F. Andersen, A. Kaplan, N. Davidson, *Phys. Rev. Lett.* **90**, 023001 (2003)
- 21 H. Katori, M. Takamoto, V.G. Pal'chikov, D. Ovsiannikov, *Phys. Rev. Lett.* **91**, 173005 (2003)
- 22 P. Treutlein, P. Hommelhoff, T. Steinmetz, T.W. Hänsch, J. Reichel, *Phys. Rev. Lett.* **92**, 203005 (2004)
- 23 A. Kaplan, M.F. Andersen, N. Davidson, *Phys. Rev. A* **66**, 045401 (2002)